THE ECONOMICAL COMPUTATION OF UNSTEADY TURBULENT FLOW STRUCTURES IN ROTATING CAVITIES

H. Iacovides, B. E. Launder and A. Zacharos
Turbulence Mechanics Group,
School of Mechanical, Aerospace and Civil Engineering,
The University of Manchester, Manchester M60 1QD, UK
h.iacovides@manchester.ac.uk

ABSTRACT

This paper reports computations of three-dimensional, unsteady turbulent flows in enclosed rotating cavities of axi-symmetric geometries, through the numerical solution of the unsteady Reynolds-averaged Navier-Stokes (URANS) equations. Three cases are computed: a co-rotating cavity with a stationary outer shroud of aspect ratio s/R=0.5; and two counter-rotating cavities of s/R=0.12, with disc speed ratios Γ of -1 (anti-symmetric) and -0.5 (asymmetric). A general-geometry flow solver is employed, with a third-order bounded discretisation scheme for convective transport and the second-order Crank-Nicolson scheme for temporal discretisation. Turbulence is modelled through the use of the high-Reynolds-number k-ε with a three-dimensional extension of an advanced, analytical wall function, used to model the effects of near-wall turbulence. In the co-rotating cavity, four pairs of stable structures are predicted around the outer part of the cavity, which rotate at half the angular speed of the discs, with the inner third in solid-body rotation. In the anti-symmetric counter-rotating cavity, fewer and more chaotic structures are predicted, with low rotational speed, but which reach the cavity centre. In the asymmetric case, the three-dimensional structures are generated from the surface of the slower disc and travel inwards, forming spirals. The resolved unsteady motion makes a substantial contribution to the overall turbulent kinetic energy. Time-averaged velocity profiles are in close agreement with corresponding experimental traverses.

1. INTRODUCTION

Flows within cavities formed between rotating discs are relevant to geophysical flows, flows between turbine discs and also to cooling flows in computer disc drives. They have been the subject of many investigations, which have been mainly confined to idealized geometries, but have included a variety of conditions. Flow conditions depend on the combinations of rotating and non- (or counter-) rotating surfaces present and also on whether there is flow through the cavity. In the absence of through-flow, the enclosed-cavity systems that have received the most attention are, Figure 1, the rotor-stator system, the co-rotating discs with a stationary outer shroud and the counter-rotating system. Owen and Rogers (1989) noted that earlier studies had assumed flow conditions to remain steady and axi-symmetric. The axi-symmetric secondary flow paths within these cavities are also shown in Figure 1. In the rotor- stator system, a single-cell structure is present, with fluid pumped outwards by the rotating disk, generating the Ekman layer and returning to the cavity centre through the Bödewadt layer along the stationary disk. In the co-rotating system, the inner region is in solid-body rotation. In the outer region, the stationary outer shroud leads to the formation of Ekman
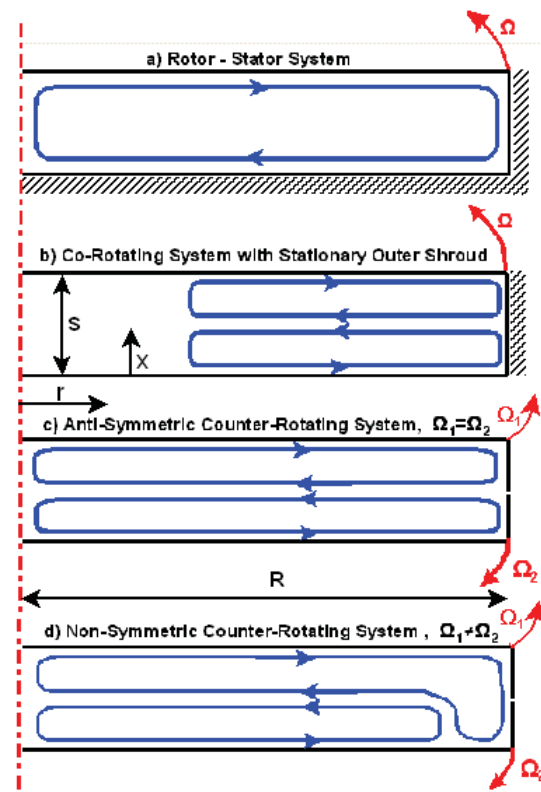

Figure 1. Schematic diagrams of axisymmetric flow fields in enclosed cavities

layers along both disks. The two Ekman layers collide at the middle of the outer shroud and form a jet directed towards the cavity centre. In counter-rotating systems, Ekman layers are again formed along both disks, while in the cavity core the fluid, which has nearly zero rotational speed, moves inwards. In contrast to the co-rotating system, these counter-rotating cells extend to the centre of the cavity. When the two disks have the same speed ($\Gamma \equiv \Omega_1/\Omega_2 = -1$), Figure 1c, the two cells are again symmetric and a stagnation point is formed at the middle of the outer shroud. When the two disks have unequal speeds, Figure 2d, the stronger Ekman layer of the faster disk spills over to the slower disk, moving the stagnation point to the outer region of the slower disk.

Until the mid-1990s it was assumed that since the boundary conditions were axisymmetric the flow would be too. However, more recent studies have shown that even in enclosed cavities with axi-symmetric geometry and boundary conditions and steady rotation, unsteady, 3-D structures can evolve. In rotor-stator systems, both DNS (Serre et al, 2001), and flow visualisation (Czarny et al.,

2002) studies, reveal unsteady 3-D structures. Videos of the latter can be accessed from the Group's website: http://tmgflows.mace.manchester.ac.uk/,

In co-rotating systems, experimental studies, Abramson et al (1991) and numerical laminar flow studies, Tucker and Long (1995), have also revealed the presence of three-dimensional structures. Inglesias and Humphrey (1998), in a numerical study, examined laminar flow in a system similar to that of Figure 2b, but with an inner hub. They showed that above a certain Reynolds number the flow becomes unsteady and three-dimensional. It is characterized by the presence of foci of intensified axial components of vorticity, distributed periodically in the circumferential direction. These foci, whose number was found to remain even and to depend on geometry and the Reynolds number, were shown to rotate at speeds ranging from 0.5 to 0.8 of the angular velocity of the system

For counter-rotating systems, the University of Bath group, Gan et al (1995) and Kilic et al (1996), provides LDA traverses, for the time-averaged velocity field. Flow visualisation studies, Szeri et al (1983) show that, for narrow-cavity counter-rotating systems, spiral patterns are present, which are Reynolds-number-dependent.

Following the strategy of Kenjeres & Hanjalić (1999) the authors' recent research efforts have focused on the use of unsteady RANS methods (URANS) to predict the 3-D time-dependent flow structures in turbulent flows in rotor-stator systems, Craft et al (2008). Turbulence was modelled using high-Re models, which, because they do not need fine near-wall meshes, allow a better resolution of the cavity core. Two alternative wall-functions were tested; the conventional, "standard", approach which assumes a log-law velocity variation across the near-wall cells and a 3-D extension of a more refined approach, Craft et al (2002), in which the near-wall velocity variation is obtained through the analytical integration of locally 1-D, boundary-layer forms of the momentum transport equations. While, with the former approach, only weak unsteadiness and simple three-dimensional flow structures were reproduced, the latter resulted in the computation of strong flow instabilities and complex flow structures. The use of high-Re turbulence models with these analytical wall functions, was thus found to be a promising route for the economical computation of 3-D unsteady flows in rotating cavities.

Here the objective is to further assess the same computational and turbulence-modelling strategy in computations of flows in co-rotating cavities with a stationary outer shroud and also in counter-rotating systems.

2.   THEORETICAL MODEL
2.1   High-Reynolds Number k-ε Model

Although modelling at eddy viscosity level within RANS is known to inadequately represent the effects of streamline curvature on turbulence, it is arguably a useful route within URANS, since the resolved unsteady motion accounts for the majority of turbulent transport. Evidence is provided by the analogous URANS studies of Rayleigh-Bénard convection by Kenjeres & Hanjalic (1999).

The unresolved turbulent stresses, are approximated through:

$$\rho\overline{u_i u_j} = \frac{2}{3}k\delta_{ij} - \mu_t\left(\frac{\partial U_i}{\partial x_j} + \frac{\partial U_j}{\partial x_i}\right) \quad (1) \quad \mu_t = \rho c_\mu \frac{k^2}{\varepsilon} \quad (2)$$

The turbulent kinetic energy, k, and its dissipation rate, ε, are obtained from the following transport equations

$$\rho\frac{\partial k}{\partial t} + \frac{\partial}{\partial x_j}\left(\rho U_j k\right) = \frac{\partial}{\partial x_j}\left[\left(\mu + \frac{\mu_t}{\sigma_k}\right)\frac{\partial k}{\partial x_j}\right] + P_k - \rho\varepsilon \quad (3)$$

$$\rho\frac{\partial\varepsilon}{\partial t} + \partial x_j\left(\rho U_j\varepsilon\right) = \frac{\partial}{\partial x_j}\left[\left(\mu + \frac{\mu_t}{\sigma_\varepsilon}\right)\frac{\partial\varepsilon}{\partial x_j}\right] + c_{\varepsilon 1}\frac{\varepsilon}{k}P_k$$
$$+ E - \rho c_{\varepsilon 2}\frac{\varepsilon^2}{k} \quad (4)$$

$$P_k = -\rho\overline{u_i u_j}\left(\frac{\partial U_i}{\partial x_j}\right) \quad (5) \quad E = 2\rho\nu\nu_t\left[\frac{\partial^2 U_i}{\partial x_j\partial x_q}\right]^2 \quad (6)$$

The E term in the ε equation, is active only in flow regions with a low local Reynolds number of turbulence, R_t [$\equiv k^2/\nu\varepsilon$] and is not usually included in high-Re k-ε models. It is added because Craft et al (2002) show that it improves predictions when high-Re models coupled to the analytical wall function are used in low turbulence flows, where, even for large near-wall cells, the normalized wall distance, y^* ($\equiv yk^{1/2}/\nu$) of the near-wall nodes falls below 30.

A further deviation from the conventional version of the high-Re k-ε is the introduction of a realizability constraint for the turbulent viscosity to ensure that (no summation):

$$\overline{u_i u_j}^2 \leq \overline{u_i^2}\,\overline{u_j^2} \qquad i\neq j \quad (7)$$

The condition is rather simplistically applied to three-dimensional flows through

$$\mu_t = \min\left(c_\mu\frac{k^2}{\varepsilon}, \frac{\frac{2}{3}k}{\max\left(\left|\frac{\partial U}{\partial y}+\frac{\partial V}{\partial x}\right|, \left|\frac{\partial U}{\partial z}+\frac{\partial W}{\partial x}\right|, \left|\frac{\partial V}{\partial z}+\frac{\partial W}{\partial y}\right|\right)}\right) \quad (8)$$

2.2   Analytical Wall-Function (AWF) Strategy

This approach, documented by Craft et al (2002), is based on an assumed eddy viscosity. A simple form is adopted in which the turbulent viscosity across the wall-adjacent cell is zero over the viscous sub-layer of thickness y_v and beyond this it increases linearly with wall distance.

$$\mu_t/\mu = 0 \qquad\qquad for\ y < y_v \quad (9)$$
$$\mu_t/\mu = c_\mu c_\ell\,(y^* \text{-} y_v^*) \qquad for\ y > y_v \quad (10)$$

the value of y_v^*, the normalised thickness of the zero μ_t layer, is determined through numerical experiments as 10.8.

The above assumed μ_t variation is then used to integrate analytically the locally 1-D transport equation of the wall-parallel momentum. The resulting velocity expression is then used to produce the value of the wall shear stress, τ_w, needed as the wall boundary condition to the discretised momentum equations over the near-wall cell.

The analytical expression for the wall-parallel velocity is subsequently differentiated to produce the variation of the velocity gradient, which then, combined with the expressions for μ_t and for P_k, produces the average generation rate of turbulence over the near-wall control volume. The near-wall variation of ε is obtained from:

$\varepsilon = 2\nu k_P/y_d^2$ for $y<y_d$ (11) $\varepsilon = k_P^{3/2}/c_l y$ for $y>y_d$ (12)

The interface value of $y_d^*=5.1$, is different from the value of 20 used in conventional wall functions, to ensure continuity of the ε variation across the two regions.

Craft et al (2002) developed the above scheme for plane flows. Within the near-wall sub-layer of a spinning disc, the velocity vector undergoes strong skewing, which such an approach is unable to reproduce. Here the AWF is extended to general 3-D flows, through the introduction of a second transport equation for wall-parallel momentum. As shown in Figure 2, in addition to the momentum equation in the direction of the resultant velocity at **n**, U_r, the wall-parallel momentum equation direction normal to that of U_r (U_t in Figure 2) is also integrated analytically. The boundary conditions for the momentum equation in direction U_r are the same as in the 2-D AWF. For the normal-velocity equation at both the wall, $y=0$, and the opposite boundary, $y=y_n$, U_t is set to zero.
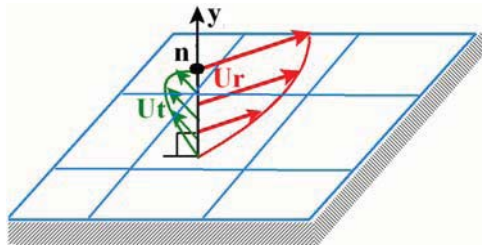
Figure 2. AWF extension to three-dimensional flows.

3.   NUMERICAL ASPECTS

Computations have been carried out using the in-house code STREAM, Lien & Leschziner (1994a), a finite-volume, general-geometry code with a collocated grid, using Cartesian velocity decomposition. The pressure is obtained through the SIMPLE algorithm. The bounded high-order UMIST scheme, Lien & Leschziner (1994b) is used for the discretisation of convection and the Crank-Nicolson scheme for temporal discretisation.

Cylindrical grids have been employed. A total of 200 planes have been used, in the circumferential direction, with 72 radial and 38 axial nodes. The number of circumferential planes was determined through grid-sensitivity tests, while the number of radial and axial nodes was arrived from similar tests but for 2-D, axi-symmetric computations. Axi-symmetric unsteady computations also suggested that a time step Δt of 0.002t is sufficient, where t is the time needed for one disc revolution.

4.   CO-ROTATING DISC FLOW

Attention is first focused on flow between two co-rotating discs and a stationary outer shroud, with aspect ratio, s/R, of 0.5 and a rotational Reynolds number, Re_Ω [$\equiv\Omega R^2/\nu$], of 1.46x10^5. Computations have been carried out for over 60 revolutions, by which point a developed 3-D unsteady field was established.

Figures 3 and 4 present a snapshot of the predicted instantaneous mean and turbulent flow fields, along the axial mid-plane of the cavity. The contours of the instant-aneous vorticity, Figure 3, show that over the inner third of the cavity the fluid is practically in solid body rotation, over the middle third conditions are close to axi-symmetric, and
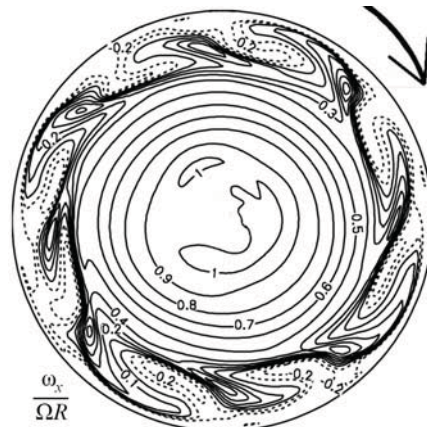

Figure 3. Contours of instantaneous, circumferential vorticity at the mid-plane (x/s=0.5) of the co-rotating cavity.
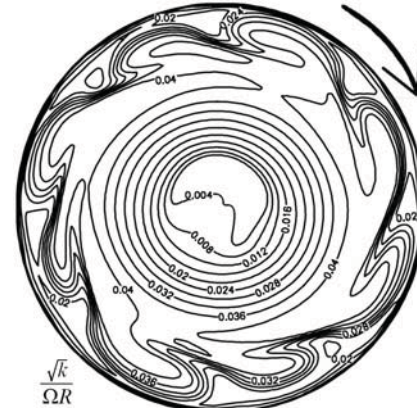

Figure 4. Contours of instantaneous, modelled turbulent kinetic energy at the mid-plane of the co-rotating cavity

over the outer third, there are four pairs of equi-spaced lobes of positive vorticity regions, surrounded by a negative-vorticity outer region. Within each pair, the leading vortex is longer than the trailing one. Flow animations, from http://tmgflows.mace.manchester.ac.uk/, show that these lobes rotate at about half the angular speed of the rotating discs. The corresponding instantaneous k contours of Figure 4 show that the inner region is a region of very low turbulence, whereas the outer 3-D structures are lobes of high turbulence.

The instantaneous flow behaviour within the radial cross-section is shown in the velocity vectors within two radial slices 45° apart, in Figure 5. They suggest that the rotating lobes in the axial plane, are caused by oscillations of the colliding wall jets (an extension of the two Ekman layers) formed around the centre-line of the outer shroud. These oscillations are repeated every 90°.

Post processing of the instantaneous field provided the time-averaged mean flow field, the resolved Reynolds stresses and also the calculation of frequency spectra at selected locations, through use of fast Fourier transforms. Figure 6 shows the power spectrum of axial velocity fluctuations, at the disc mid-plane, x/s=0.5. The frequency is non-dimensionalised through the Strouhal number, defined as $St \equiv f t$, where f is the frequency. In the outer region, the dominant frequency of the axial velocity fluctuations is at a Strouhal number of just over 2. This is consistent with the observed flapping of the plane jet, along the outer shroud, which goes through a complete period over an angle of 90°,
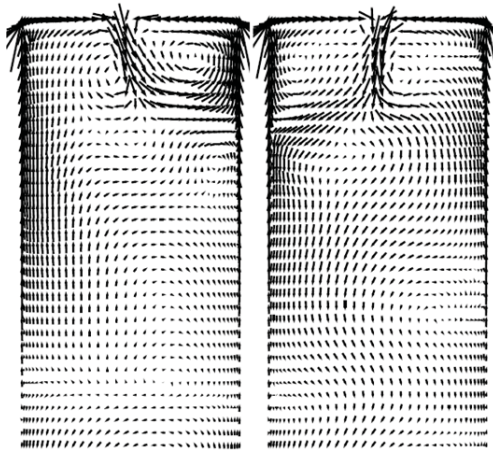
Figure 5. Vector plots of the instantaneous velocity within radial slices at 45° intervals, for the co-rotating cavity.

while rotating at about half the angular speed of the discs. Further, smaller peaks on either side of the dominant frequency suggest the presence of unsteady flow structures with a range of scales. Over the inner half of the cavity (not included), the higher frequency components disappear, leaving the dominant frequency at St near 0.9.

The influence of flow unsteadiness on turbulence, is examined through the profiles of the time-averaged turbulence intensity, in Figure 7, and the contribution made by the modelled and resolved components. The former is the time-averaged value of k, obtained from the solution of the k equation and represents the contribution of the small-scale fluctuations, not resolved with URANS. The latter, is obtained by statistically post-processing the instantaneous velocity field and represents the contribution of the large-scale motion resolved by URANS. The profiles show that near the outer shroud, r/R=0.85, both components make sizeable contributions to the overall k, though close to the discs the modelled levels are higher. In the middle part of the cavity, r/R=0.55, the two components have similar magnitudes near the discs, but the resolved component gradually drops to very low levels in the core, while the modelled contribution reaches a plateau. Thus the overall turbulence level, which is what is recorded in experiments, can be higher, by a factor of 2 in places, than the modelled component, returned by steady RANS simulations.
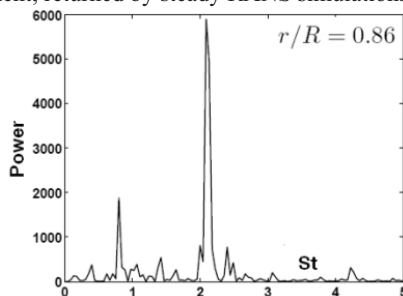

Figure 6. Power spectrum of axial velocity fluctuations, at the disc mid-plane, x/s=0.5, for co-rotating cavity

5, COUNTER-ROTATING DISC FLOWS

Here two cases of flow between counter-rotating disks are examined, for which Gan et al (1995) provide traverses of the time-averaged velocity. In both cases the aspect ratio
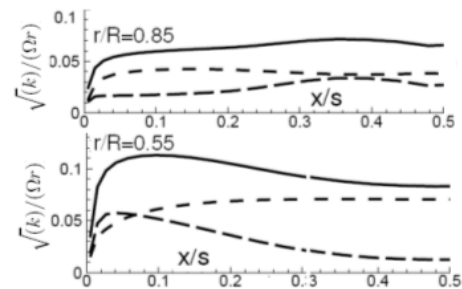

Figure 7. Time-averaged turbulence intensity across the cavity, for co-rotating case. ------- : modelled component, __ __ __ : resolved component ____ : resultant component

s/R, is 0.12 and the rotational Reynolds number, based on the angular velocity of the faster disc, is 10^5. There is no inner hub and the outer shroud is divided into two equal halves, each attached to one of the discs. In the first, the anti-symmetric, case, the two discs rotate at equal and opposite speeds. The dimensionless ratio, Γ ($\equiv \Omega_1/\Omega_2$), is thus -1. The second case is non-symmetric, with the slower disc rotating at half the speed of the other, Γ=-0.5.

5.1 Anti-symmetric case, Γ = -1

As shown in Figure 1, as in the co-rotating case, the two Ekman layers meet along the outer shroud, where they collide and form a radial jet directing fluid towards the cavity centre. These similarities suggest that for the anti-symmetric case, it would be reasonable to expect that flow instabilities will originate along the outer shroud. The plots of the instantaneous turbulence intensity fields within axial planes, shown in Figure 8, do confirm this feature. The high turbulence regions suggest that a number of vortices are present along the cavity outer region. Moreover, closer to the disc surfaces, x/s=0.95, these vortices become stronger than in the cavity mid-plane, x/s=0.5. These unsteady structures are, however, neither as large, nor as regular as in the co-rotating cavity, shown in Figures 3 and 4 and, as already pointed out, the fluid in the cavity core has very low angular velocity, so these structures do not rotate around the cavity. Plots of the instantaneous flow field within radial sections, Figure 9, provide further evidence of the irregular nature of the three-dimensional flow structures in this counter-rotating system. The vorticity plots of Figure 9 show a flapping motion along the outer shroud, with structures shed and carried to the cavity centre. Corresponding contours of the instantaneous turbulence intensity (not included), show that turbulence is generated along the outer shroud, where the Ekman layers collide. Figure 10 shows the power spectrum of the axial velocity fluctuations, at the disc mid-plane, x/s=0.5. In the outer region, r/R=0.9, most fluctuations are confined to Strouhal numbers less than 1, with the primary peaks at St<0.5. These frequencies are lower than those observed in the co-rotating cavity. This is consistent with the fact that in the co-rotating case more structures are formed around the perimeter and that these structures also rotate at about half the discs angular velocity. In the counter-rotating case there are fewer structures and their rotational speed is very low. Closer to the centre of the cavity, (not included here) while the frequency spectrum remains the same, there is a considerable reduction in the peak levels.
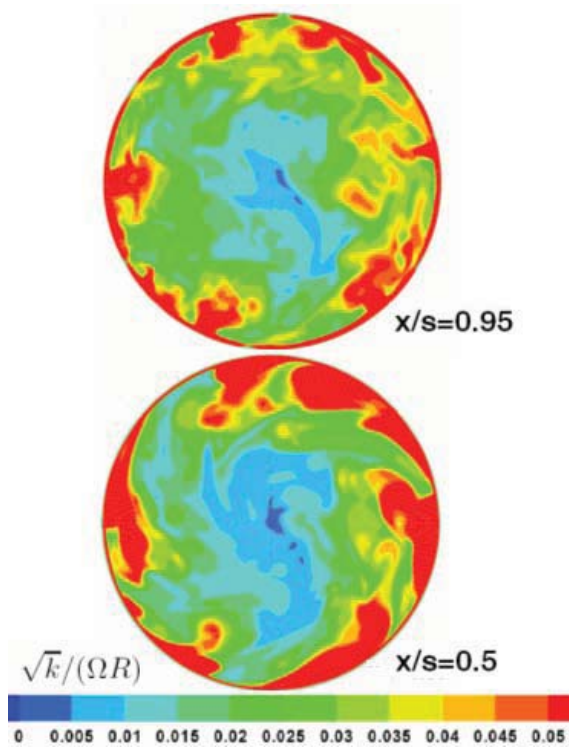
$\sqrt{k}/(\Omega R)$ x/s=0.5

Figure 8. Contour plots of instantaneous modelled turbulence intensity field, in axial planes, for counter-rotating disc cavity, at $\Gamma = -1$.

5.1 Asymmetric case, $\Gamma = -0.5$.

As shown in Figure 1, the imbalance between the two Ekman layers, moves, their point of collision to the outer region of the slower disc. Since, in the previous cases this stagnation point has been the source of instabilities, it is to be expected that the origin of such instabilities will now be displaced to the surface of the slower disc. The contours of instantaneous vorticity over two different axial slices, Figure 11, confirm this. Close to the slower disc, x/s=0.75, a number of spiral structures are present, which originate
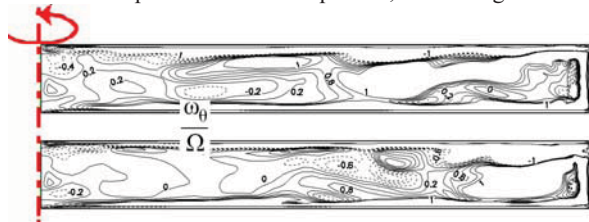

Figure 9. Contours of instantaneous vorticit in radial planes, at 45° intervals, for counter-rotating disc cavity, at $\Gamma = -1$.

from a ring close to the outer shroud and extend towards the cavity centre. The strength of these spiral structures is progressively reduced across the cavity, from the slower to the faster disc. Corresponding turbulent kinetic energy contours, (not included) also show spiral structures along the slower disc and indicate that turbulence levels along the slower disc are higher than those along the faster surface. The contour plots of instantaneous vorticity within radial
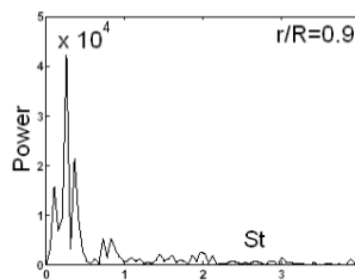

Figure 10. Power spectrum of axial velocity fluctuations, at the disc mid-plane, for counter-rotating cavity, Γ=-0.5.

cross-sections, Figure 12, provide further evidence that flow instabilities originate along the slower disc, for $r/R \approx 0.9$, which is where the two Ekman layers collide. These contour plots also show that the structures shed from the stagnation point travel towards the centre of the cavity. Because they also have a rotational component in their motion, this gives rise to the spiral traces observed in Figure 11.
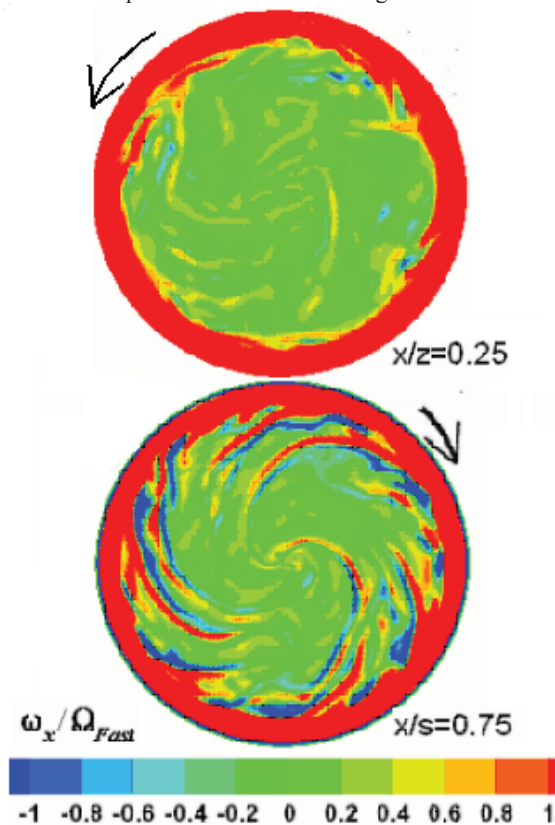

Figure 11. Contours of the instantaneous, circumferential vorticity along the axial planes of the counter-rotating cavity, for Γ=0.5, with x/s=0 the surface of the faster disc.

Finally, it is also instructive to compare profiles of the time-averaged velocity produced by the 3-D URANS, with measurements and those of 2-D RANS. Figure 13, compares measurements by Gan et al (1995) with predicted profiles of the time-averaged radial velocity. The present computations (Fig.12a) are in reasonably close agreement with the experimental data at all locations, including r/R=0.85 and r/R=0.8, which are close to the stagnation point along the slower disc. The thickness of the boundary layers and the peak levels of the near-wall radial velocity
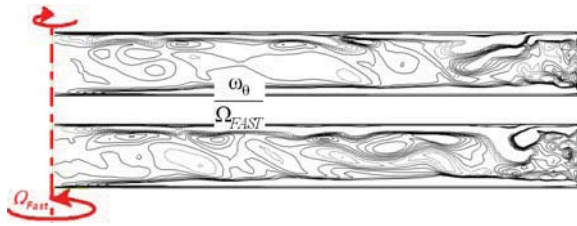
Figure 12. Contours of instantaneous vorticity, within radial planes, at 45° intervals. Counter-rotating cavity, at $\Gamma = -0.5$.

are well reproduced. The 2-D RANS predictions of Iacovides at al (1996), on the other hand, show marked differences between the low-Re k-ε computations and the measurements, especially in the outer region of the cavity. Along the faster disc, the peak value of the radial velocity is under-estimated. Along the slower disc, the negative values of the near-wall radial velocity indicates that, 2-D RANS computations, predict the stagnation point at $r/R < 0.8$, while the experimental data and also the 3-D URANS, suggest that the stagnation point is located at $r/R > 0.85$.
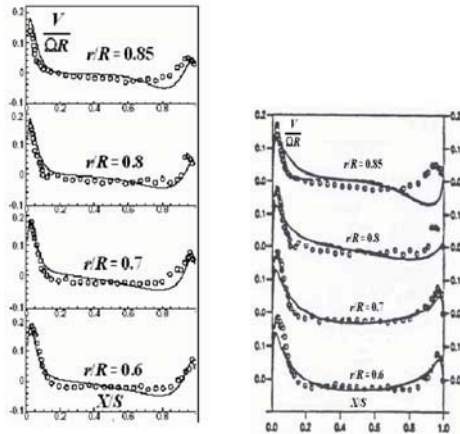
a) Present 3-D URANS   b) 2-D RANS Iacovides et al (1996)

Figure 13. Time-averaged radial velocity in a counter-rotating cavity, $\Gamma = -0.5$, —— Computations: o o o : Expt. Gan et al (1995)

6.   CONCLUDING REMARKS

The 3-D URANS approach has been used to compute flow in three different types of enclosed rotating cavities, in which the time-averaged flow field involves a two-cell structure within the radial cross-section with Ekman layers on both discs. Flow instabilities originate at the point of collision of the two Ekman layers. The 3-D URANS approach, with a modelling strategy involving, high-Re turbulence models and a 3-D form of an analytical wall function, provides an effective and economical numerical tool for the simulation of large-scale flow instabilities.

In the co-rotating disc case, in common with earlier laminar flow studies, the 3-D URANS return solid-body rotation near the cavity centre, nearly axi-symmetric flow at the middle and four pairs of regularly spaced vortical structures around the outer third, which rotate at about half the speed of the discs. In the anti-symmetrically counter-rotating cavities, flow instabilities are also generated along the outer shroud, but the 3-D structures are fewer and more chaotic than in the co-rotating case, have very low angular

speed and reach the centre of the cavity. In the asymmetrically counter-rotating cavity, flow instabilities originate along the slower disc and form a set of spirals.

Comparisons show that, in certain regions, the resolved fluctuations make similar contributions to the overall turbulent kinetic energy as their modelled counterpart. Frequency analysis of the resolved fluctuations suggests that in the co-rotating cavities, where the 3-D structures are regular and repeatable, most of the energy of the resolved unsteady motion is concentrated at a few distinct frequencies. In the counter-rotating cases, where the 3-D structures are more chaotic, the energy of the resolved motion is more evenly spread over a range of frequencies

The time-averaged flow obtained by post-processing the 3-D URANS data, is in close agreement with experimental data. For the asymmetric counter-rotating case, velocity profiles from 3-D URANS are closer to the measurements than those of 2-D simulations. This suggests that large-scale 3-D structures have a strong enough effect on the flow to influence the time-averaged behaviour.

REFERENCES

S. M. Abrahamson J.K. Eaton and D. J. Koga, 1991, "The flow between shrouded co-rotating disks", *Phys Fluids A,* **1:** 241-251

T. J. Craft, A Gerasimov, H. Iacovides and B.E. Launder, 2002, "Progress in the generalization of wall-function treatments.", *Int. J. Heat & Fluid Flow*, **23**:148-16.

T. J. Craft, H. Iacovides, B.E. Launder and A Zacharos, 2008, "Some Swirling-flow Challenges for Turbulent CFD", *Fl., Turb. & Combustion*, **80**: 419-434.

O. Czarny, H. Iacovides and B. E. Launder, 2002, "Precessing Vortex Structures in Turbulent Flow within Rotor-Stator Disc Cavities.", *Flow, Turb. & Comb.,* **69**: 51-61.

X. Gan, M. Kilic, and J.M. Owen, 1995, "Flow between contra-rotating disks.". *J. Turbomachinery*, **117**: 298–305.

H. Iacovides, K.S.Nikas, and M. Te Braak, , 1996, "Turbulent flow computations in rotating cavities using low-Reynolds number models." Paper No *ASME-96-GT-159 , Int. Gas-Turb & Aero Congress*, Birmingham, UK.

I. Inglesias I and J.A.C Humphrey, 1998, "Two- and three-dimensional laminar flows between disks co-rotating in a fixed cylindrical enclosure.", *Int. J. Num. Meth. Fluids,* **26**:581–603.

S. Kenjeres and K. Hanjalic, 1999, "Transient analysis of Rayleigh-Benard convection with a RANS model." *Int. J. Heat & Fluid Flow*, **20**:329–340.

M. Kilic, X. Gan, and J.M. Owen, 1996, "Turbulent flow between two disks contra-rotating at different speeds", *J. Turbomachinery*, **118**: 408–413.

F-S Lien and M. A. Leschziner 'A general non-orthogonal finite-volume algorithm for turbulent flow at all speeds incorporating 2ⁿᵈ moment turbulent transport closure" *Comp Meth Appl Mech Eng*, **114**: 123-167

F-S. Lien and M.A. Leschziner, 1994b, "Upstream monotonic interpolation for scalar transport with application to complex turbulent flows.", *Int. J. Num. Meth. Fluids*, **19**:527–548.

J.M. Owen and R.H. Rogers, 1989, "Flow and Heat Transfer in Rotating-Disc Systems.", Vol 1 *John Wiley & Sons.*.

E. Serre, E. Crespo del Arco, and P. Bontoux, 2001. "Annular and spiral patterns in flow between rotating and stationary discs.", *J. Fluid Mech*, **434**:65–100.

A.Z. Szeri, A. Giron, S.J. Schneider, and H.N. Kaufman, 1983, "Flow between rotating disks. part 2: stability.", *J. Fluid Mechanics,* **134**:133–154.

P.G. Tucker and C.A. Long, 1995," Numerical investigation into influence of geometry, on flow in a rotating cavity with an axial through flow.", *Int. Comn. Heat Mass Transfer*, **22**:639–648.